Simultaneous Accurate Polarization Measurement with Three Wavelengths with a Color Polarization Camera

Manal Altaweel , Judit Bisbal-Amat , Juan Campos * , Ángel Lizana , Irene Estévez

Posted Date: 23 April 2026

doi: 10.20944/preprints202604.1686.v1

Keywords: optical polarization; Stokes parameters; polarization cameras

Article

Simultaneous Accurate Polarization Measurement with Three Wavelengths with a Color Polarization Camera

Manal Altaweel, Judit Bisbal-Amat, Juan Campos *, Ángel Lizana and Irene Estévez

Group of Optics at the Department of Physics of the Universitat Autònoma de Barcelona

* Correspondence: juan.campos@uab.cat

Abstract

Polarimetric color cameras are a forefront technology that simultaneously capture polarimetric and color information by analyzing polarization states across different color channels, commonly red, green, and blue. In general, each of these color channels can carry different polarization information. Therefore, measuring the polarization Stokes vector at several discrete wavelengths simultaneously and with the highest possible resolution is of interest in multiple research areas. Nonetheless, this situation has not yet been investigated in specialized literature, where it is still commonly assumed that all color channels transport the same polarization information. In practice, polarimetric color cameras often come with the difficulty of color filter overlapping. For instance, the green filter partially transmits red and blue wavelengths, causing polarization-color crosstalk. In this work, we present a method to solve this problem. In addition, Fourier domain demosaicing techniques are applied to interpolate the data and reconstruct the images. The present study demonstrates how the proposed method leads to a successful recovery of chromatic and polarimetric information on both synthetic and real-world datasets. To test our approach, narrowband light beams at three wavelengths (470, 554, 630 nm), with different spatial polarization and degree of linear polarization distributions have been simulated and validated with experimental data. The results demonstrate the feasibility of the method for accurate three polarization channels measurements.

Keywords: optical polarization; Stokes parameters; polarization cameras

1. Introduction

Some fundamental physical quantities associated with light are intensity, wavelength, phase, and polarization. With regards to polarization, polarimetric imaging techniques have become an excellent tool not only for enhanced vision applications, but also for revealing information which remains hidden in other non-polarimetric imaging methods. Typically, this means recording the full or partial Stokes vectors of light across an image plane [1]. Applications of polarization imaging include remote sensing [2], astronomy [3], applications in industry [4], biophotonics [5], machine vision [6] and general contrast enhancement [7]. Thus, enhancements to polarimetric systems may significantly contribute to the advancement of the aforementioned fields.

The concept of a sensor that images the amount and angle of polarization at each pixel and in one image was introduced in 1994 by Chun [8]. This technique is now commonly known as microgrid polarimetric imaging (MPI). It is dedicated to division-of-focal plane (DoFP) polarimeters, which enables the analysis of the direction of the light's electric field oscillation. The emergence of DoFP image sensors represents a significant milestone in the evolution of polarization imaging, offering a versatile and efficient means of capturing polarization information in real-time, without the complexities associated with traditional polarization imaging techniques [9,10].

A set of independent polarization sensitive measurements (four as minimum) are required for the full Stokes vector determination of a light beam. Before the arrival of MPI, this situation was

 doi:10.20944/preprints202604.1686.v1

typically achieved by complex setups [11], or time-sequential configurations [12], which made such characterization procedure based on bulky systems or time-consuming, respectively. These limitations prevented the polarization systems from being implemented in real-time applications. However, the emergence of MPI devices enabled the acquisition of spatial information while overcoming these limitations, using sensors consisting of ordered arrays of four-polarization based macro-pixels. Consequently, this novel technology has attracted considerable interest in applications requiring rapid measurement of structures with spatially varying polarization.

Additionally, a valuable approach for imaging applications is to combine spectroscopic and polarimetric information, which can be beneficial for image enhancing and automatic classifications purposes [13]. Under this scenario, some authors have presented configurations able to integrate the advantages of DoFP and integral field spectroscopy to implement a linear- Stokes imaging spectropolarimeter [14]. Moreover, recent achievements in image sensor manufacturing technology have given rise to novel RGB polarimetric cameras [15], built with single-chip polarized color sensors, capable of capturing simultaneously both RGB and polarization data in a mosaic form. The typical architecture of these sensors comprises arrays of super-pixels, organized as groups of 4 × 4 pixels, including blocks of four directional polarizers (typically at angles of 0◦, 45◦, 90◦ and 135◦), each one associated with a different color filter (Red, Green, Green and Blue, resulting in RGGB-type polarimetric cameras). Note that featuring RGGB color filters and directional polarizing filters, leads to distinctive 12-pixel units, forming the required RGGB-Polarization pattern (see an example in the illustration shown Figure 1). Under these conditions, by properly processing information provided by polarimetric color cameras, the linear content of the Stokes image associated with a given scene, at three different wavelengths, can be retrieved.

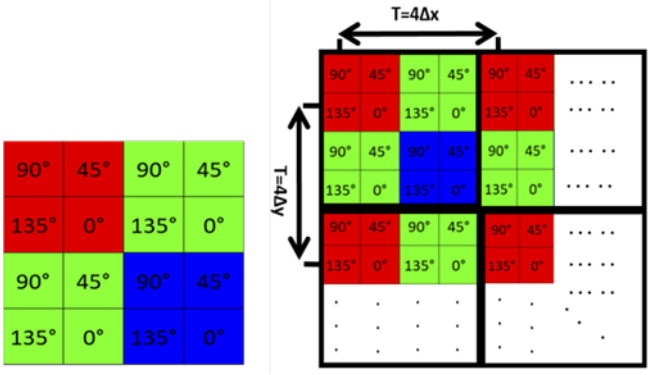

Figure 1. (left): The unitary pixel cell (or super pixel). (right): The full polarimetric color sensor consists of repeated 12 different analyzers (super pixel) following a periodic pattern. The closer pixel of the same class is found at distances 4·Δx and 4·Δy.

Despite its many benefits, there are some limitations to consider. On the one hand, polarimetric cameras sacrifice spatial resolution to form the stated super-pixels. To overcome this situation, the use of interpolation algorithms becomes mandatory [16]. On the other hand, the inclusion of RGGB polarimetry snapshot sensors typically involves color crosstalk between filters, which can introduce errors in the measurement process, leading to inaccuracies in determining the polarization state of light. Thus, the implementation of a color crosstalking removal method is required. Both problems have been addressed separately, and some solutions have been provided for interpolation of polarimetric cameras alone [17] as well as for crosstalking of spectroscopic channels alone [18,19]. In addition, in [20] the authors face the problem of using wide band spectral illumination and non-achromatic retarders, and they propose a robust calibration method. However, in this paper we address another problem. We want to measure accurately the polarimetric response of samples when using three nearly monochromatic light sources simultaneously. The wide band transmission of the Bayern filters produces a crosstalk between the color channels which can lead to significant errors in

 doi:10.20944/preprints202604.1686.v1

the determination of the Stokes vectors distribution carried out by the three wavelengths. Here, we propose a method to solve this problem.

The structure of this work is organized as follows: Section 2 presents the mathematical formalism used to model color-polarimetric cameras. Section 3 discusses the theoretical formulation of the measurement model, and the method for removing color crosstalk is described. Section 4 details the simulation results, and Section 5 the experimental validation. Finally, the conclusion summarizes the key findings and implications of the study.

2. Materials and Methods

2.1. Color Polarimetric Camera Model

As previously stated, the polarimetric color camera consists of 12 different analyzers, considering the four different linear polarizations and the three-color filters. The unitary pixel cell (or super-pixel) containing the 12 analyzers is represented in Figure 1(left). To complete the camera sensor, this super pixel is replicated over the full sensor following a periodic pattern. Under this scheme, if an individual pixel has a size of Δx and Δy in the x and y directions respectively, when considering a particular pixel class, the closer pixel of the same class is found at distances 4·Δx and 4·Δy respectively (see Figure 1(right)). Consequently, for a camera sensor with (NxN) pixels dimension, the 12 polarimetric images obtained by using the polarimetric color camera present a N/4 x N/4 dimension, and thus, presents a reduced resolution compared to the camera sensor resolution. Under this scenario, to fill in the information in empty data spaces, we should apply an interpolation process to obtain smoother intensity images before being used for Stokes calculation purposes. After the interpolation, we will have 12 (NxN) images, each one corresponding to a specific combination of polarizer orientation and a color filter.

2.2. Mathematical Formalism of Color-Polarimetric Cameras Model

The polarimetric response of a sample, such as biological tissue, depends on the illuminating wavelength. Thus, using more than one color to inspect a sample is likely to provide additional information about it. Our aim is to illuminate the samples with three wavelengths simultaneously and measure the polarization for all three colors. To this end, we use three LEDs with interferential filters that have spectral bandwidths of about 10 nanometers, and central wavelengths of 630nm, 554nm, and 470nm. However, the spectral color band of the Bayern filters in the camera are very broad, causing the information carried out by the different wavelengths to overlap. This leads to color crosstalk effects, where polarization signals from different colors overlap. We propose a method to mitigate this effect and ensure accurate separation and measurement of polarimetric and color information. This section is devoted to providing a method able to reduce the crosstalk effect associated with color polarimetric cameras.

We now introduce a measurement model to address the issue of color crosstalk that occurs between the different color channels in images obtained by the camera. Let $\vec{S}^{\lambda}(x,y), \lambda = \lambda_1, \lambda_2, \lambda_3$ be the three polarization distributions (Stokes vectors) corresponding to the three wavelengths used. In each pixel, there is one of the four polarization analyzers, corresponding to the orientation of the micro polarizers. In addition, as mentioned above, each pixel is covered by a different color filter that exhibits some transmission for each of the three wavelengths. Let (t_f^{λ}) be the intensity transmission of a color filter "f" for a wavelength "l". Let $\vec{A}_p^{\lambda}$ be the analyzer corresponding to one of the four-polarizer orientation "p" for a wavelength "l". Then, given a pixel with a polarizer orientation "p" in front of a color filter "f" illuminated with a wavelength "l", the resulting intensity $\left(I_{pf}^{\lambda}\right)$ will be:

$$I_{pf}^{\lambda} = t_f^{\lambda}(\vec{A}_p^{\lambda})\vec{S}^{\lambda} = t_f^{\lambda} I_p^{\lambda}. \quad (1)$$

 doi:10.20944/preprints202604.1686.v1

If the three wavelengths work at the same time, the resulting intensity will be:

$$I_{pf}^{ct} = \sum_{\lambda} I_{pf}^{\lambda} = \sum_{\lambda} t_f^{\lambda}(\vec{A}_p^{\lambda})\vec{S}^{\lambda} = \sum_{\lambda} t_f^{\lambda} I_p^{\lambda} . \quad (2)$$

Note that I_{pf}^{ct} are the intensities we obtain after interpolating the intensity measurements. Moreover, the super-index *ct* indicates that these intensities are affected by crosstalk. Therefore, to obtain the three polarization distributions we should be able to get the intensity distributions I_p^{λ} by solving (2). This equation can be rewritten in a matrix form as follows:

$$I_{pf}^{ct} = CI_p^{\lambda}, \quad (3)$$

where C is the transfer matrix relating I_p^{λ} with I_{pf}^{ct}, I_p^{λ} being the original intensity distribution corresponding to the polarizer orientation "p" and wavelength "λ", and the measured distribution affected by the cross talk.

To solve (3) the matrix C must be experimentally calibrated. Thus, we have measured the transmission intensities of the three-color filters for our case. In particular, our experiment deals with a polarimetric RGGB camera by Lucid Vision, which is equipped with a Sony IMX250MYR CMOS sensor.

To calculate the transmission intensities of the RGB color filters, we illuminated the camera with one wavelength at a time, using either left or right circularly polarized light. In this way, the intensity transmitted by the camera polarizers does not depend on their orientation. These measurements can also be done with fully unpolarized light. The results are arranged in Table 1.

Table 1. Relative intensities transmissions of RGB filters.

		Wavelength		
		R (630nm)	G (554nm)	B (470nm)
Transmission	R-filter	1	0,04	0,01
	G-filter	0.25	1	0,19
	B-filter	0,03	0.10	0,72

Considering the experimental transmission intensities given in Table 1, the relation given by (3) can be written in a matrix form as:

$$\begin{pmatrix} I_{1,1}^{ct} \\ I_{2,1}^{ct} \\ I_{3,1}^{ct} \\ I_{4,1}^{ct} \\ I_{1,2}^{ct} \\ I_{2,2}^{ct} \\ I_{3,2}^{ct} \\ I_{4,2}^{ct} \\ I_{1,3}^{ct} \\ I_{2,3}^{ct} \\ I_{3,3}^{ct} \\ I_{4,3}^{ct} \end{pmatrix} = \begin{pmatrix} 1 & 0 & 0 & 0 & 0{,}04 & 0 & 0 & 0 & 0.01 & 0 & 0 & 0 \\ 0 & 1 & 0 & 0 & 0 & 0{,}04 & 0 & 0 & 0 & 0{,}01 & 0 & 0 \\ 0 & 0 & 1 & 0 & 0 & 0 & 0{,}04 & 0 & 0 & 0 & 0{,}01 & 0 \\ 0 & 0 & 0 & 1 & 0 & 0 & 0 & 0{,}04 & 0 & 0 & 0 & 0{,}01 \\ 0.25 & 0 & 0 & 0 & 1 & 0 & 0 & 0 & 0.19 & 0 & 0 & 0 \\ 0 & 0.25 & 0 & 0 & 0 & 1 & 0 & 0 & 0 & 0.19 & 0 & 0 \\ 0 & 0 & 0.25 & 0 & 0 & 0 & 1 & 0 & 0 & 0 & 0.19 & 0 \\ 0 & 0 & 0 & 0.25 & 0 & 0 & 0 & 1 & 0 & 0 & 0 & 0.19 \\ 0.03 & 0 & 0 & 0 & 0.1 & 0 & 0 & 0 & 0.72 & 0 & 0 & 0 \\ 0 & 0.03 & 0 & 0 & 0 & 0.1 & 0 & 0 & 0 & 0.72 & 0 & 0 \\ 0 & 0 & 0.03 & 0 & 0 & 0 & 0.1 & 0 & 0 & 0 & 0.72 & 0 \\ 0 & 0 & 0 & 0.03 & 0 & 0 & 0 & 0.1 & 0 & 0 & 0 & 0.72 \end{pmatrix} \begin{pmatrix} I_{1,1} \\ I_{2,1} \\ I_{3,1} \\ I_{4,1} \\ I_{1,2} \\ I_{2,2} \\ I_{3,2} \\ I_{4,2} \\ I_{1,3} \\ I_{2,3} \\ I_{3,3} \\ I_{4,3} \end{pmatrix}. \quad (4)$$

By inverting this equation, we can obtain the intensity distributions without crosstalk:

$$I_p^{\lambda} = C^{-1} I_{pf}^{ct} . \quad (5)$$

3. Results

This section may be divided by subheadings. It should provide a concise and precise description of the experimental results, their interpretation, as well as the experimental conclusions that can be drawn.

 doi:10.20944/preprints202604.1686.v1

3.1. Data interpolation

As we have mentioned when describing the camera, each intensity measurement corresponding to a given combination of polarization orientation and color filter is acquired at different spatial locations, resulting in a loss of spatial resolution. To obtain a full-resolution intensity image for a particular color-polarization combination, we should perform some kind of interpolation. In this work, we have used the Fourier-domain interpolation, which is the best option for band limited signals [19]. For the discussion in this paper the type of interpolation is not crucial. This represents the first step to acquire the intensities I_{pf}^{ct}, which still contain crosstalk effects.

3.2. Polarization and crosstalk analysis. Simulated data

In this subsection we analyze the proposed method to mitigate crosstalk and to measure the spatial polarization distribution in the three-color channels simultaneously. To this end, we simulate a scenario in which each wavelength transports different spatial polarization information. To describe the polarization state, we use three parameters (the intensity is assumed equal to one): Degree of polarization (DoP), Azimuth (Az) and Ellipticity (El). The corresponding components of the Stokes vector will be given by

$$\begin{cases} S_0 = 1 \\ S_1 = DoP * cos(2El) * cos(2Az) \\ S_2 = DoP * cos(2El) * sin(2Az) \\ S_3 = DoP * sin(2El) \end{cases}. \quad (6)$$

Since we are measuring linearly polarized light, the ellipticity (El) is set equal to 0. The three linear partially polarized light spatial distributions corresponding to each wavelength are defined as:

1. RED Wavelength: The DoP varies with the radial coordinate between 0.5 and 1; the azimuth varies with the angular coordinate between -180 and 180 degrees.
2. GREEN Wavelength: The DoP varies with the radial coordinate between 0.5 and 1; the azimuth varies with the X coordinate.
3. BLUE Wavelength: The DoP is a correlated random distribution, and the azimuth varies with the Y coordinate.

In the first simulation, we assume that there is no crosstalk, let us say, the elements outside the diagonal in Table 1 are equal to 0. Figure 2 summarizes the results obtained for the GREEN channel. The left column presents the Azimuth (Az) (first row) and Degree of Linear polarization (DoLP) (second row) parameters of the original functions. The central column shows the differences between the original and the reconstructed parameter after the intensity interpolation and polarimetric data reduction. Finally, the right column shows the histograms of these differences.

 doi:10.20944/preprints202604.1686.v1

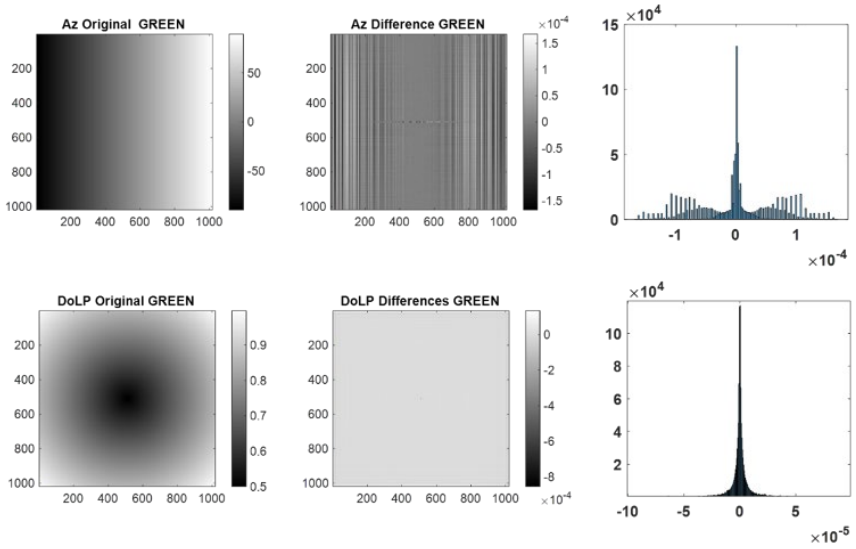

Figure 2. GREEN Channel, NO crosstalk. The first row corresponds to the Azimuth and the second to the DoLP. The Left column corresponds to the original function. The central column is the error (difference between the original function and the interpolated and the reconstructed one). The right column is a histogram of the corresponding error.

As one can see from Figure 2, the errors are almost negligible, with magnitudes on the order of 10-4. The oscillations in the azimuth errors are due to the discontinuity between the left and right borders when using Fourier Transform interpolation.

In the next simulation, we assume that there is crosstalk between color channels, as described in Table 1, which is then corrected using the method described in (4). The reconstruction results can be seen in Figure 3. The resulting errors are of the same order of magnitude as those obtained in the absence of crosstalk, indicating an accurate performance of the method proposed for crosstalk correction.

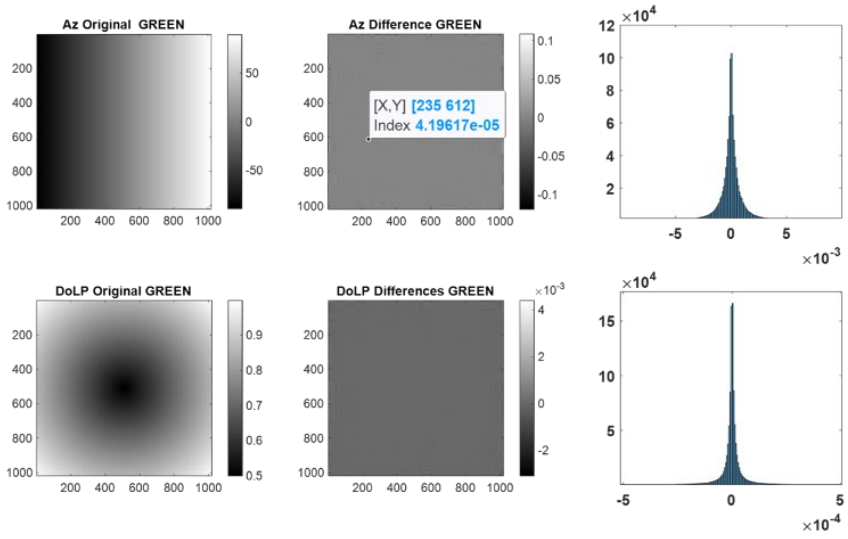

Figure 3. GREEN Channel, WITH corrected crosstalk. The first row corresponds to the Azimuth and the second to the DoLP. The Left column corresponds to the original function. The central column is the error (difference between the original function and the interpolated and the reconstructed one). The right column is a histogram of the corresponding error.

Finally, we have made the simulation with crosstalk, but when it is not corrected in the reconstruction. The results are shown in Figure 4 for the GREEN channel.

 doi:10.20944/preprints202604.1686.v1

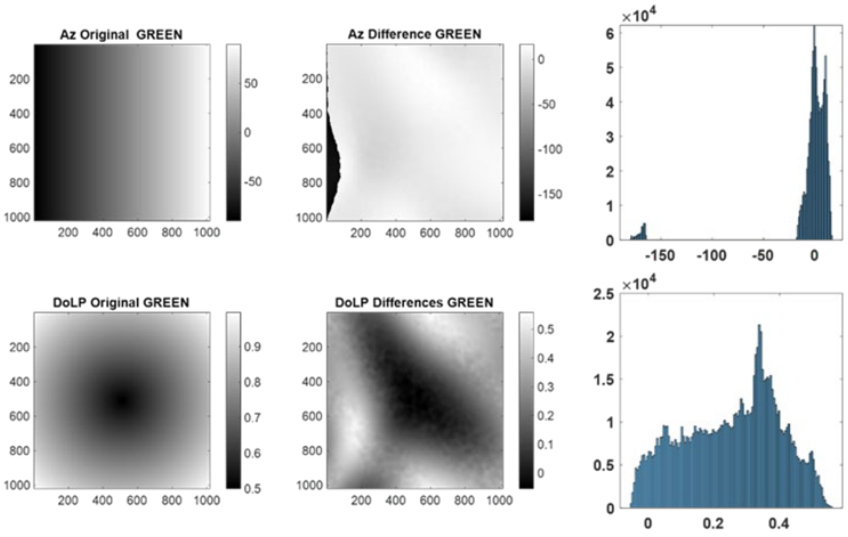

Figure 4. GREEN Channel, with NON-corrected crosstalk. The first row corresponds to the Azimuth and the second to the DoP. The Left column corresponds to the original function. The central column is the error (difference between the original function and the interpolated and the reconstructed one). The right column is a histogram of the corresponding error.

As we can see in this figure, the errors in the azimuth of the green channel are much larger than in the previous case with crosstalk correction. The error in the DoLP could reach up to 50% on the green channel. This shows the need to correct the crosstalk to accurately measure with three wavelengths simultaneously.

3.3. Polarization and crosstalk analysis. Experimental results

To validate the method with experimental results we have performed the following experiment: a radial polarizer (from Codixx) with 8 sectors is followed by a non-achromatic wave plate, so, at the exit of the system, different elliptical polarizations are obtained for each sector and for each wavelength. The setup is illuminated sequentially with red, green, and blue wavelengths and measurements are taken. After that, we illuminated simultaneously with the three wavelengths. In this case, we assume that the beams are fully polarized, so, by knowing (S0, S1, S2) we can compute the S3 component as,

$$S_3 = \sqrt{S_0^2 - S_1^2 - S_2^2}\ . \qquad (7)$$

As said above, the combination of a linear polarizer with different orientations and the waveplate produces different elliptical polarizations (azimuth and ellipticity) for each sector. Furthermore, because the wave-plate is not achromatic, these parameters will be also different for each wavelength. To avoid prolonging the discussion, only the green channel results are displayed in Figure 5 since in the experiments it is the channel presenting the most significant error regarding the crosstalk effects.

 doi:10.20944/preprints202604.1686.v1

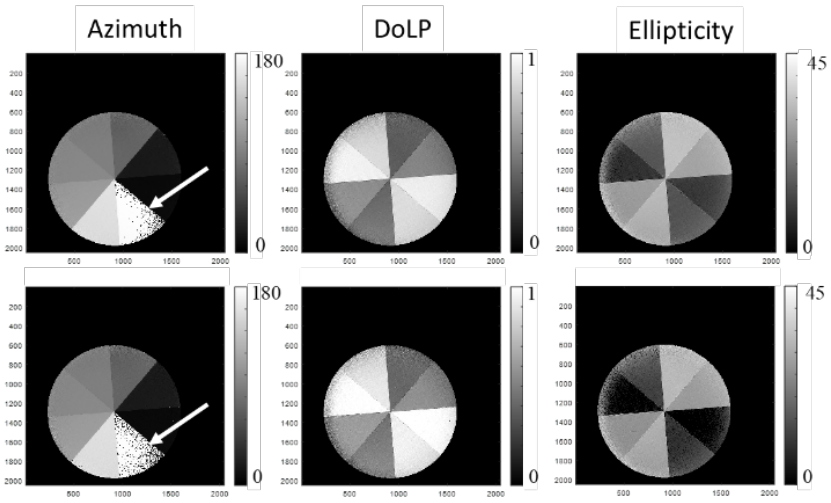

Figure 5. GREEN channel after interpolation and crosstalk correction. (Top row) system illuminated only with the green wavelength. (Bottom row) system illuminated with the tree wavelengths. (Left) Azimuth, (Center) DoLP, (Right) calculated Ellipticity.

Top row of Figure 5 shows the results obtained after interpolation and crosstalk correction for the green channel when the system is illuminated only with the green wavelength. Bottom row of the figure shows the same results obtained when the system is illuminated with the three wavelengths at once.

The left column shows the azimuth of the obtained elliptical polarizations. Note that 0º and 180º correspond to the same azimuth although they are displayed in black or white, as can be seen on the bottom right sector (see white arrow). Each sector combined with the waveplate produces different ellipse orientations. The same results are obtained either with one or three wavelengths illuminating, showing that the proposed method is working well.

As we are measuring only with linear polarizers, only the components (S0, S1, S2) can be measured, and then all the elliptical parts of the polarization produce linear depolarization. The Degree of Linear Polarization (DoLP) is shown in the central column of the figure to illustrate this effect. When the polarizer of a sector is parallel to the axis of the waveplate, the produced polarization will be linear, and the DoLP will be almost 1, while in the other cases the DoLP will decrease, with the limit case of ellipticities close to 45º, leading to the lowest DoLP values. Again, we can see that the top and bottom figures give the same results.

Finally, the column on the right shows the evaluated ellipticity assuming that light is fully polarized by using (7). We can see that when the DoLP is near to 1, the ellipticity is near to 0. We want to note that a major contribution of the method is that we can measure simultaneously with three different wavelengths that after interacting with the sample produce different polarization distributions. As a representative example, we also include the experiment performed with the green channel and presented in Figure 5, but now applied to the blue channel. The corresponding results are shown in Figure 6. Because the blue illumination has a shorter wavelength, the retrieved ellipticity values become more pronounced compared to the green case, which in turn leads to lower DoLP values. Note that the results obtained when using a single wavelength illumination, or three wavelengths simultaneously are equal.

 doi:10.20944/preprints202604.1686.v1

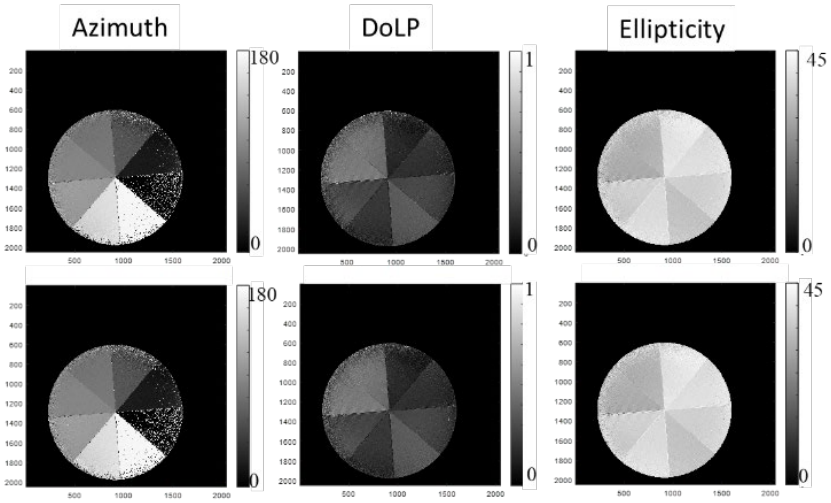

Figure 6. BLUE channel after interpolation and crosstalk correction. (Top row) system illuminated only with the blue wavelength. (Bottom row) system illuminated with the tree wavelengths. (Left) Azimuth, (Center) DoLP, (Right) calculated Ellipticity.

4. Discussion

In this paper, we are assuming that different wavelengths carry out distinct polarization distribution after interacting with a sample. The color polarization cameras give an opportunity to measure in a single shot the polarization distributions carried out by the three wavelengths. There are two issues that must be solved to obtain accurate measurements: the sampling of the signals and the crosstalk between the color channels.

Each polarization/color combination is measured in different spatial locations. Then, to accurately calculate the polarization state, interpolation is needed. We have selected the interpolation in the Fourier domain because it is the best according to the sampled signal theory for band limited functions. Only when there are abrupt changes in intensity that produce very high frequencies, will the errors be significant at these edges.

In the color cameras, the color filters have very wide bandwidth producing crosstalk between the color channels, i.e. the green filter also has nonzero transmission for the red and blue wavelengths. We have measured the relative transmission of each of the color filters, and with this information we have proposed a method to correct the crosstalk, being able to determine the intensity distribution for each of the three wavelengths.

The method has been experimentally validated by measuring different samples presenting different polarization spatial distributions and for three wavelengths. We have demonstrated that it is possible to measure the polarization distributions simultaneously and accurately at three different wavelengths, thereby reducing the total measurement time by a factor of three.

Author Contributions: Investigation, M. Altaweel; Conceptualization, J. Campos; validation, J. Bisbal-Amat; writing—original draft preparation, M. Altaweel.; writing—review and editing, A. Lizana and I. Estévez.; supervision, J. Campos, A. Lizana, I. Estévez.; All authors have read and agreed to the published version of the manuscript.

Funding: This work was supported by the Ministerio de Ciencia e Innovación and Fondos FEDER (Ref. PID2024-156240OB-C22).

Conflicts of Interest: "The authors declare no conflicts of interest.".

Data Availability Statement: data underlying the results presented in this paper may be obtained from the authors upon request.

 doi:10.20944/preprints202604.1686.v1

Abbreviations

The following abbreviations are used in this manuscript:

DoFP	Division-of-Focal Plane
MPI	Microgrid Polarimetric Imaging

References

1. Serres, J.R.; Lapray, P.J.; Viollet, S.; *et al.*, "Passive polarized vision for autonomous vehicles: a review," *Sensors* **24**(11), **3312** (2024). https://doi.org/10.3390/s24113312
2. Tyo, J.S.; Goldstein, D.L.; Chenault, D.B.; and Shaw, J.A. "Review of passive imaging polarimetry for remote sensing applications," *Appl. Opt.* **45**(22), 5453–5469 (2006). https://doi.org/10.1364/AO.45.005453
3. Snik, F. and Keller, C.U. "Astronomical polarimetry: polarized views of stars and planets," in *Planets, Stars and Stellar Systems*, T. D. Oswalt and H. E. Bond, eds. (Springer, Dordrecht, 2013). https://doi.org/10.1007/978-94-007-5618-2_4
4. Mériaudeau, F.; Ferraton, M.; Stolz, C. J. ; *et al.*, "Polarization imaging for industrial inspection," *Proc. SPIE* **6813**, **681308** (2008). https://doi.org/10.1117/12.767915
5. Rodriguez, C.; van Eeckhout, A.; Ferrer, L.; et al., "Automatic pseudo-coloring approaches to improve visual perception and contrast in polarimetric images of biological tissues," *Sci. Rep.* **12**(1), 18479 (2022). https://doi.org/10.1038/s41598-022-23330-6
6. Estévez, I.; Oliveira, F.; Braga-Fernandes, P.; et al., "Urban objects classification using Mueller matrix polarimetry and machine learning," Opt. Express 30, 28385–28400 (2022). https://doi.org/10.1364/OE.451907
7. Venkatesulu, E.; Buglione, K.L.; Field, N.J.; et al., "Polarization enhancement of contrast through a water surface," Appl. Opt. 64(6), 1443–1453 (2025). https://doi.org/10.1364/AO.544390
8. Chun, C.S.L. ; Fleming, D.L.; and Torok, E.J. "Polarization-sensitive thermal imaging," Proc. SPIE 2234, 275–286 (1994). https://doi.org/10.1117/12.181025
9. Ratliff, B.M.; Tyo, J.S.; Rodríguez-Herrera, O.G.; and Alenin, A.S. "Angle of polarization confidence metric for polarization imaging," *In Polarization: Measurement, Analysis, and Remote Sensing XVI*, Proc. SPIE 13050, 1305002 (2024). https://doi.org/10.1117/12.3012968
10. Rodríguez-Herrera, O.G.; Tyo, J.S.; Wang, L. *et al.*, "Feasibility analysis and Mueller matrix retrieval strategy for a scene-adaptive modulated imaging polarimeter," *Polarization Science and Remote Sensing XI*, Proc. SPIE 12690, 148-156 (2023). https://doi.org/10.1117/12.2676575
11. X. Lv, X.; Zhu, S. ; Guo, X. *et al.*, "Full-Stokes polarimetric light-field imaging using only a single detector," *Opt. Lasers Eng.*, ., 129, 106071. (2020). https://doi.org/10.1016/j.optlaseng.2020.106071
12. Gendre, L.; Foulonneau, A. and Bigué, L. "High-speed imaging acquisition of Stokes linearly polarized components using a single ferroelectric liquid crystal modulator," *Polarization Science and Remote Sensing IV*, Proc. SPIE 7461, 74610G (2009). https://doi.org/10.1117/12.826403
13. Pierangelo, A.; Manhas, S.; Benali, A. et al., "Multispectral mueller polarimetric imaging detecting residual cancer and cancer regression after neoadjuvant treatment for colorectal carcinomas," J. Biomed. Opt. 18(4), 046014 (2013). https://doi.org/10.1117/1.JBO.18.4.046014
14. Mu, T.; Pacheco, S.; Chen, Z.; et al. "Snqapshot linear-Stokes spectropolarimeter using division-of-focal-plane polarimetry and integral field spectroscopy", Sci Rep. 2017;7:42115. https://doi.org/10.1038/srep42115
15. "LUCID Camera," *ThinkLucid Technical Briefs*. https://thinklucid.com/tech-briefs/polarization-explained-sony-polarized-sensor/
16. Ratliff, B.M.; LaCasse, C.F.; and Tyo, J.S. "Interpolation strategies for reducing IFOV artifacts in microgrid polarimeter imagery," *Opt. Express* **17**(11), 9112–9125 (2009). https://doi.org/10.1364/OE.17.009112
17. Liu, J.; Duan, J.; Hao, Y. et al., "Polarization image demosaicing and RGB image enhancement for a color polarization sparse focal plane array," *Opt. Express* **31**, 23475-23490 (2023). https://doi.org/10.1364/OE.494836
18. Qiu, S.; Fu, Q.; Wang, C.; and Heidrich, W., "Linear polarization demosaicing for monochrome and color polarization focal plane arrays," *Comput. Graph. Forum* 40(6), 77–89 (2021). https://doi.org/10.1111/cgf.14204

 doi:10.20944/preprints202604.1686.v1

19. Hagen, N.; Stockmans, T.; Otani, Y. and Buranasiri, P., "Fourier-domain filtering analysis for color-polarization camera demosaicking," Appl. Opt. 63, 2314-2323 (2024). https://doi.org/10.1364/AO.516696
20. Li, H.; Bian, S.; and Arteaga, O. "Robust calibration method for polarization cameras integrated with chromatic retarders," Opt. Express 33, 31155-31166 (2025). https://doi.org/10.1364/OE.566847
21. Goldstein, D.H., *Polarized Light*, 3rd ed. (CRC Press, 2017). https://doi.org/10.1201/b10436
22. Goodman, J.W., *Introduction to Fourier Optics*, 3rd ed. (Roberts & Company, 2005). https://doi.org/10.1063/1.3035549